Title of Publication *Edited by*
TMS (The Minerals, Metals & Materials Society), Year

A 3D GRANULAR MODEL OF EQUIAXED-GRANULAR SOLIDIFICATION

A.B. Phillion, J.-L. Desbiolles, and M. Rappaz

Computational Materials Laboratory
Ecole Polytechnique Fédérale de Lausanne
CH-1015 Lausanne, Switzerland

Keywords: Aluminum Alloys, Solidification, Granular Model, Hot Tearing

Abstract

The solidification of an aluminum-copper alloy has been simulated in 3D using a granular model. Compared to previous similar 2D approaches for where only one phase is continuous, the extension to 3D allows for concurrent continuity of the solid and liquid phases. This concurrent continuity is a key factor in the formation of the solidification defect known as hot tearing. In this 3D model, grains are modeled as polyhedrons based on a Voronoi tessellation of a pseudo-random set of nucleation centers. Solidification within each polyhedron is calculated using a back-diffusion model. By performing a series of simulations over a range of grain sizes and cooling rates, the percolation of the solid grains is determined. The results, which indicate that the grain size and cooling rates play an important role in hot tear formation, constitute a basis on which feeding and deformation calculations will be carried out further.

Introduction

During the casting of metallic alloys, the semi-solid material is frequently exposed to a tensile stress state due to temperature gradients and mechanical constraints. These tensile stresses often lead to the formation of hot tears, or solidification cracks [1, 2]. This defect represents the formation of a large crack in the still semi-solid casting, and generally requires rejection of the entire cast part. Hot tears occur at the end of the solidification interval, when continuous liquid films surround the solid grains and yet there is a lack of interdendritic liquid feeding. These tears are intergranular in nature with a few solid spikes resulting from deformation of solid bridges or solidification of the last liquid [3, 4].

While much hot tearing research has been performed, both experimentally and modeling-wise (see review by Eskin *et al.* [5]), the formation of a hot tear has yet to be reliably simulated [6]. The best of the available criteria can predict only the probability of hot tearing as a function of casting parameters, not the formation of a hot tear itself. Hot tearing predictions are inherently challenging, due to the stochastic distribution of the liquid and solid phases, and the stochastic arrangement of large numbers of grains during solidification. Unfortunately, most of today's models have focused on averaging methods at the macro-scale (*e.g.* [7, 8]), which do not contain any information about the solid and liquid phase repartition. While other techniques provide this information, such as the phase field (or equivalent) methods, they are limited to the scale of only a few grains. An intermediate and interesting approach is a microstructure model based on granular structures, in which the properties of both phases can be utilized while simulating a large number of grains in an efficient and quick manner.

Granular structures have previously been used to model material behaviour during the solidification process. Early models assumed a regular arrangement of grains to describe semi-solid ductility [9] and liquid feeding [10]. However, this geometry does not approximate solidification very well since the solid grains do not become interconnected until the volume

fraction of solid, g_s, is equal to 1. Recently, a 2D solidification model has been developed by Vernède *et al.* [11, 12] using granular structures, but based on geometry derived from a Voronoi tessellation. The use of a Voronoi tessellation provides for stochastic variability in the grain size, grain shape, and hence the surrounding liquid topology. This model simulates solidification by advancing the grain edges towards the border along linear segments which connect the nuclei with Voronoi vertices, taking into account back-diffusion and thermodynamic coalescence at the grain boundaries. The results of such 2D models show that the localization of liquid feeding begins at g_s ~0.97. Phillion *et al.* [13] have also developed a semi-solid model based on Voronoi-type granular structures. Instead of modeling solidification, this granular model was used to predict the constitutive behavior of semi-solids at a specific fraction solid and grain sizes via a direct finite element (FE) simulation of solid grains surrounded by an interconnected liquid.

While the granular solidification model by Vernède *et al.*, and the granular semi-solid deformation model by Phillion *et al.* show promise in resolving some of the issues relating to hot tearing, their 2D formulation is a key shortcoming. This is because in 2D, either the solid or liquid phase can be continuous through the domain for a specific fraction solid, but not both. In reality, simultaneous continuity of both phases occurs. This results in both larger and longer-lasting liquid films. In the present work, a granular solidification model is extended to 3D. The first part of the paper contains a description of the model formulation. In the second part of the paper, the 3D granular model is compared to the previously-developed 2D model. Finally, the 3D model is applied to show the effects of cooling rate and grain size on solidification behavior. These simulations were performed for an Al-1wt%Cu alloy with a grain size of 100 μm and a cooling rate of -1 K/s, unless otherwise stated.

Model Formulation

The 3D granular solidification model is an extension of the 2D model developed by Vernède *et al.* [11, 12]. The model is based on a Voronoi tessellation of random nucleation centers for providing realistic grain sizes and shapes within a fixed Representative Volume Element (RVE). A Voronoi tessellation is a methodology for determining the domain closest to a given nucleation center rather than any other. In 2D, these polygonal domains have an arbitrary number of edges and vertices, depending on the configuration of the nuclei. In 3D, the polyhedral domains consist of an arbitrary number of polygonal faces, edges, and vertices. Each polyhedron represents one fully solid grain after complete solidification, if the grain growth is assumed to be globular. It has previously been shown that if the thermal gradient is small then the final grain structure predicted by a Voronoi tessellation is similar to the grain structure predicted by more computationally intensive methods, such as phase field [12].

The size of the RVE is dependent on both the grain density and grain size, and is given by:

$$\ell_{RVE} = N_g^{1/3}\bar{d} \tag{1}$$

where $\bar{d}$ is the average grain diameter, N_g is the number of grains, and ℓ_{RVE} is the length of one side of the RVE; $\bar{d}$ and N_g are model input parameters. The grain nuclei are placed randomly inside the RVE subject to the constraint that the minimum permissible distance between any two nuclei is one third of the grain size. Thus, although the grain nuclei are randomly placed within the RVE, the grain nuclei are dispersed with some ordering to create well-shaped grains.

After construction of the Voronoi tessellation, solidification in each grain is carried out by advancing a planar front from the nucleation center to each of the polygonal faces using a micro-segregation model. In order to simplify the solidification model, each grain is divided into pyramids having the nucleation center as the summit and the polygonal face as its base. These pyramids are further divided into tetrahedral elements, by subdividing each polygonal face into triangles. This division of geometry is shown in Figure 1, for a REV with 27 grains, 227 faces, and 1674 tetrahedral elements. Thus, even small numbers of grains will contain many elements, with only these elements playing a role in the calculations. The four nodes of each tetrahedron

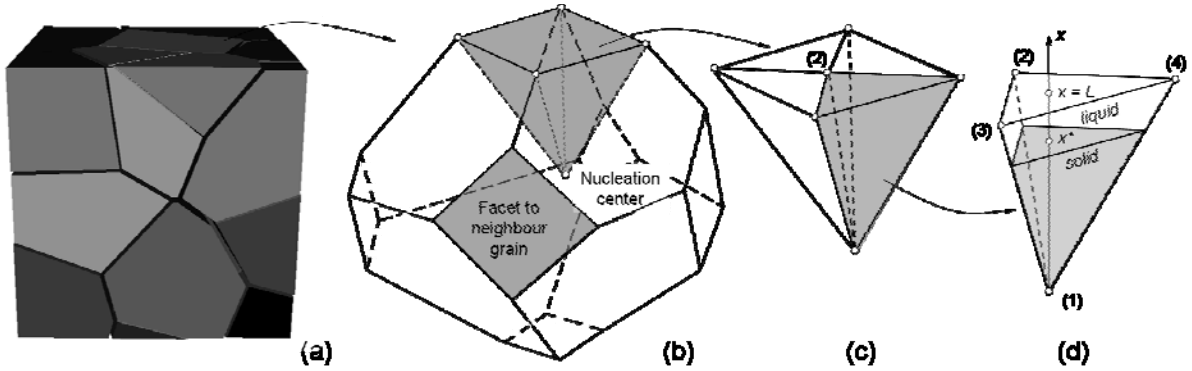

Figure 1: A breakdown of the REV geometry making up the 3D granular solidification model – (a) the entire model domain; (b) a polyhedral grain; (c) a pentahedral volume element; (d) a single tetrahedral element showing both the solid portion (grey) and liquid portion (clear).

(Figure 1d) are: (1) the grain nucleation center, (2) the centroid, and (3),(4) two neighbor vertices of the polyhedral facet. Since this geometry is created using a Voronoi tessellation, each tetrahedral element will share nodes 2–4 with a symmetric element from a neighboring grain.

The model is based on solidification occurring within each tetrahedral element only, and with no solute flux between elements. Thus, solidification in each tetrahedron can be reduced to a one-dimensional problem, assuming complete diffusion in the liquid and back-diffusion in the solid. The volume fraction of solid in each tetrahedron is given by $g_s = \left(x^* / L\right)^3$, where x^* is the position of the solid-liquid interface, and L is the height of the tetrahedron measured from the nucleation centre (Figure 1d). While the previous 2D models have included grains with rounded corners based on the Gibbs-Thompson effect [12], this rounding becomes quite complex in 3D and has not yet been included in the current model, *i.e.* the grains remain polyhedral.

The master equation controlling the evolution of the solid-liquid interface can be derived from a solute balance integrated over the liquid phase of the tetrahedral element:

$$v^* x^{*2}\left(k-1\right)C_l + \frac{1}{3}\left(L^3 - x^{*3}\right)\frac{dC_l}{dt} + x^{*2} D_s \left.\frac{\partial C_s}{\partial x}\right|_{x^*} = 0 \qquad (2)$$

where v^* is the velocity of the interface, k is the partition coefficient, and D_s is the diffusion coefficient in the solid. The term $\frac{dC_l}{dt}$ can be replaced with $\frac{\dot{T}}{m}$, where $\dot{T}$ is the cooling rate (°C s^{-1}) and m is the slope of the liquidus line, since concentrations at the solid-liquid interface are imposed by the phase diagram and complete mixing in the liquid has been assumed. The evolution of the term $\left.\frac{\partial C_s}{\partial x^*}\right|_{x^*}$ is solved using a finite difference scheme of the diffusion equation in the solid phase and a Landau transformation to follow the interface [14].

At the end of solidification, two grains may become mechanically in contact, but will not be thermodynamically in contact due to the excess energy of the various interfaces involved (solid-liquid, and solid-solid). Rather, as introduced by Rappaz *et al.* [15], a thin layer of liquid will remain until a sufficient undercooling is achieved to overcome this excess surface energy. This coalescence undercooling between two grains is a function of both the relative grain orientation, and the thickness of the liquid layer. Coalescence effects are felt when the liquid film thickness is on the order of the diffuse solid-liquid interface thickness (d ~5 nm). Coalescence plays a large role in hot tearing since undercoolings on the order of 75°C as compared to the equilibrium liquidus can be achieved, extending the temperature range where continuous liquid films exist prior to final solidification. Hence, it has been implemented into the 3D granular model in a manner similar to its implementation in the 2D model [11]. Once this coalescence undercooling has been overcome, the liquid film disappears and grain coalescence has occurred.

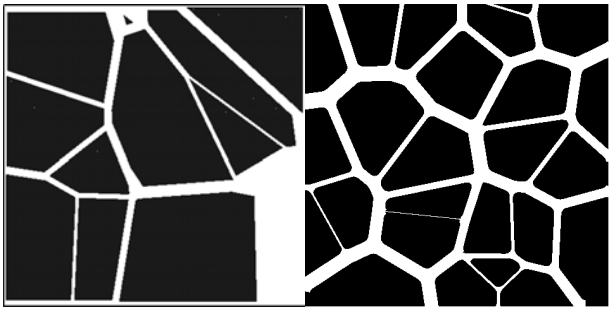

(a) (b)

Figure 2: A comparison of the two granular models for $g_s \cong 0.75$; (a) 3D and (b) 2D.

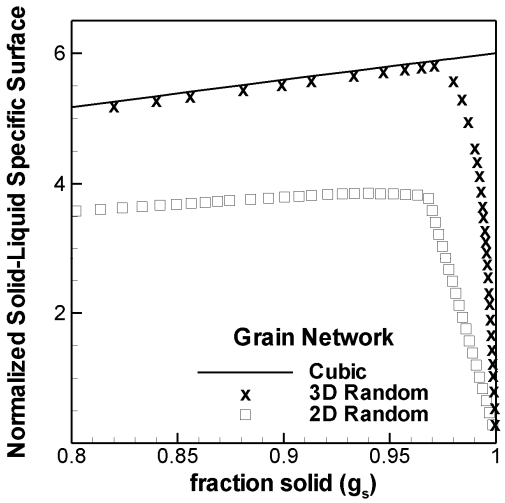

Figure 3: S_v^0 as a function of g_s for the 2D and 3D granular models. The theoretical curve for a regular series of cubic grains is also shown.

Comparison of the 2D and 3D Model Predictions

Figures 2 and 3 show a comparison of the granular solidification model predictions for the 2D and 3D geometries at $g_s \cong 0.75$. In Figure 2, a cross-sectional slice of the 3D model (2a), and an image of the 2D model (2b) are provided. These images show clearly the locations of the liquid (white) and solid (dark) phases. In Figure 3, the evolution of the solid-liquid surface area, S_v^o, as a function of g_s is shown for both models. S_v^0 is defined as the solid-liquid surface area divided by the RVE volume, and multiplied by the grain size [11]. The theoretical curve for a regular arrangement of cubic grains is also given.

As can be seen in Figure 2, the liquid remaining in between the grains in the 2D simulation consists of fairly regular liquid channels. In the cross-section of the 3D simulation, the average thickness of the liquid channels is slightly reduced, but large regions where liquid exists can remain. This is because the 3D model contains a liquid network with substantial connectivity; whereas only a few channels, on the order of 4 or less, can be connected at the vertices in the 2D model. The large liquid region in Figure 2a is a result of the cross-sectional slice being cut exactly through a liquid channel. The presence of these large liquid regions is important for prediction solidification defects. With respect to porosity, the liquid provides a large source of hydrogen and a minimum nucleation barrier for pore formation. With respect to hot tearing, the large regions of liquid can act both as sources to improve liquid feeding, but also reduces the effective solid-solid surface area in response to applied load. The 2D model, with only small liquid channels, cannot capture these effects.

As can be seen in Figure 3, the evolution of the normalized solid-liquid interfacial area, S_v^0, is dependent on both dimension and geometry. This quantity is important when discussing the transition from a continuous liquid network, to a continuous solid network in the mushy zone. The theoretical curve for a regular arrangement of cubic grains is given by $6g_s^{2/3}$, whereas that for a 2D regular cubic network is given by $4g_s^{1/2}$. Since coalescence occurs in all the cubic grains at $g_s = 1$, S_v^0 continues to increase until $g_s = 1$; it then falls abruptly to zero. The figure shows that the 3D random network follows the theoretical curve until $g_s \cong 0.975$, when a maximum is reached and the curve begins to fall smoothly to zero. At this value of g_s, the decrease in S_v^0 due to grain coalescence is larger than the increase in S_v^0 due to the increase in fraction solid. Although the 2D curve is quite different from the 3D curve in both absolute values and in the slope, its maximum also occurs at $g_s \cong 0.975$ but with a model using rounded grain corners (the rounded grain corners results in less liquid on the edges but more liquid at the triple points). Hence, in terms of coalescence, the two models are similar. However, liquid cannot pass at all in the 2D model once two grains have coalesced, whereas the liquid can go around in the 3D model, due to the addition of the extra dimension.

Results

3D Granular Solidification

Figure 4 shows the type of result that can be obtained from the 3D granular solidification model. Although the simulations have been run with as many as 8000 grains, the images shown here contain only 27 grains for good image quality. Figure 4a provides the calculated evolution in fraction solid with temperature, while Figures 4b–4f are images showing the variation in 3D grain morphology with increasing fraction solid.

The fraction solid – temperature relationship calculated by the 3D granular solidification model shows typical behavior for low-concentration alloys. Firstly, there is a considerable increase in fraction solid in the early stages of solidification. Secondly, the last liquid solidifies over an extremely long temperature range. In this case, for Al-1wt%Cu, the final five percent of the liquid solidifies over a temperature range of 120°C, which is five times as large as the temperature range for the first ninety-five percent of solidification.

As can be seen in the images 4b–4f, the grains begin as small crystals (4b, 4c) growing within the melt. At g_s = 0.5 (4d), the grains have become sufficiently large that a liquid network is beginning to form. With a further increase in fraction solid (4e), the liquid network begins to hold great importance with flow only possible along specific liquid channels to feed the solidification shrinkage and mushy zone deformation. Finally, at very high fraction solid (4f) the grains begin to coalesce and form a coherent structure. This sequence of solidification is similar to prior research [16, 17], except that it is not sufficient to simply look at the development of the solid network. The structure of the liquid network also plays an important role in the

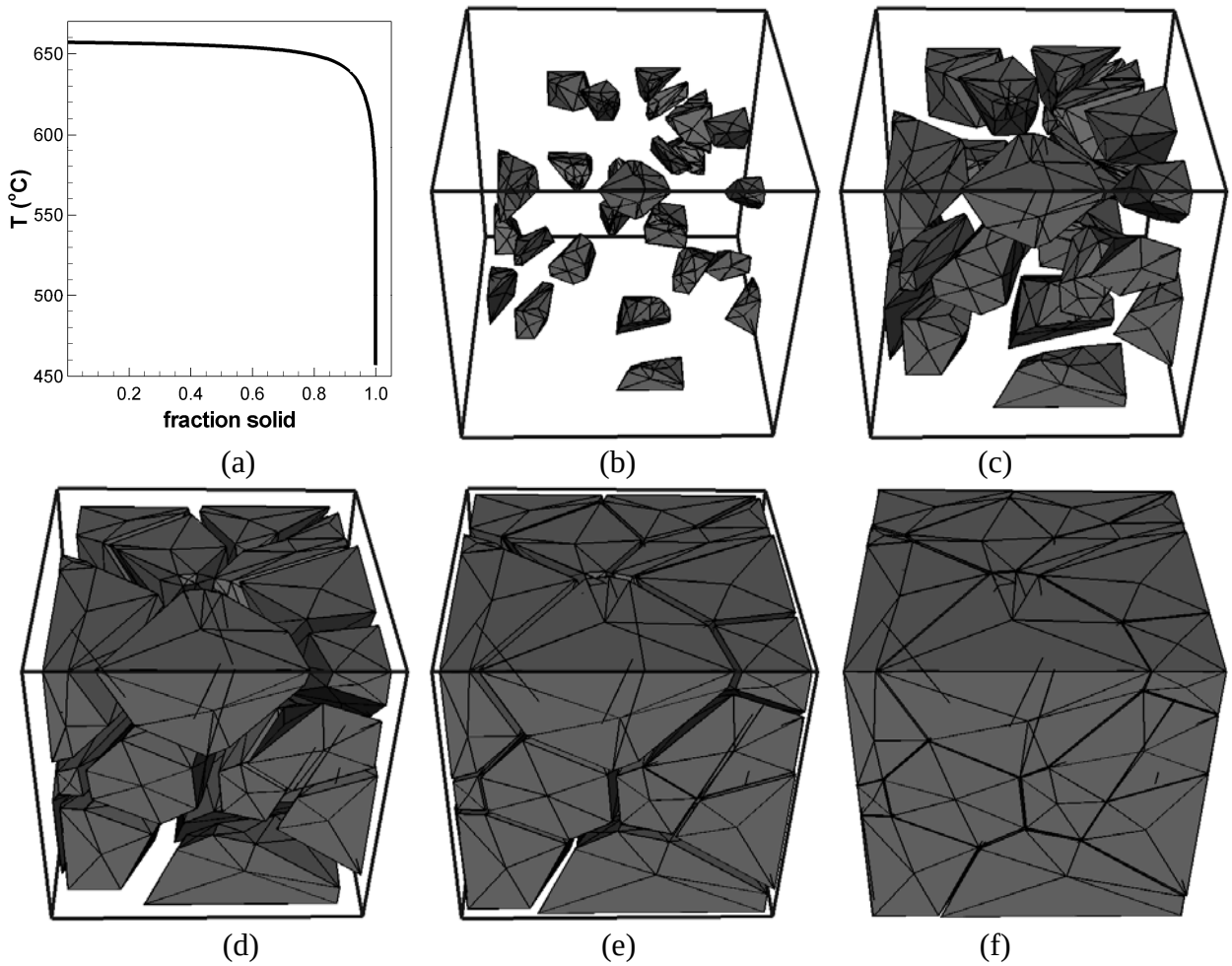

Figure 4: Solidification sequence for a 27 grain 3D granular solidification model –
(a) Evolution of g_s with temperature;
(b)-(f) Images showing 3D structure for increasing g_s (0.02, 0.15, 0.50, 0.80, 0.95).

solidification sequence. Indeed, the solid network does not develop until very high fraction solid, while the liquid network is continually changing in size and structure.

At a given fraction solid, the width of an individual liquid channel is mainly a function of the distance between two nuclei. The closer the nuclei, the smaller the liquid channel. With increasing fraction solid, the smaller channels close and coalesce while the larger channels continue to exist. This selective coalescence occurs due to the inclusion of back-diffusion within the solid phase, and would not occur using the lever or Scheil rules for solidification. Compared to these models, which are functions of temperature only, back-diffusion adds an important length-scale to solidification via the Fourier number. In Figure 4, the distance between two nuclei ranges from 30 μm to 280 μm for $\overline{d}$ = 100 μm. Thus, although $\overline{d}$ is fixed, the use of a Voronoi tessellation results in a large range of grain sizes. This variation in grain size is similar to the variation found in industrial castings [18].

The phenomenon of selective coalescence depending on the size of the liquid channels leads to the formation of grain clusters, with a cluster being defined as a continuous solid. In Figure 4, the domain begins with 27 clusters since there are 27 grains, and then decreases down to 1 cluster after solidification is completed. The evolution of solidification clusters is linked to both the distance between two nuclei and the cooling rate, and can only be captured by a granular solidification model due to the stochastic nature of random nuclei placement. The formation of such clusters is critical in predicting hot tearing since it affects the degree to which both thermally-induced strain and liquid feeding are localized within the mushy zone.

Based on the observations of Figure 4, the 3D granular solidification model provides insight into two critical mushy zone features. The first is the fraction solid at which a continuous solid network develops within the RVE, and the second is the evolution in the cluster density as a function of the fraction solid. These features, discussed below, were investigated by performing a series of 1000-grain solidification simulations over a range of grain sizes and cooling rates.

Percolation of the Solid and Liquid Phases

In Figure 5, the fraction solid for percolation, $g_{s,perc}$, has been plotted as a function of cooling rate for four different grain sizes –25, 50, 100, and 200 μm. Percolation is defined as the fraction solid when there is a continuous path of solid from one side of the RVE to the other side. At this value of g_s, many of the grains are in physical contact after coalescence. In a 2D model, the remaining liquid can be continuous only along a path more or less parallel to the continuous solid path. However, in a 3D model, the liquid can remain as a percolated phase even in a direction perpendicular to the first percolated solid path. While some of the remaining liquid exists as isolated pockets, the 3D model has shown that the liquid phase will remain percolated virtually until g_s=1. In terms of solidification, $g_{s,perc}$ is important since a percolated semi-solid is able to resist the tensile deformations that lead to hot tearing. Hence, castings with a lower value of $g_{s,perc}$ will tend to have improved hot tearing resistance because feeding will be made easier when deformation of the solid skeleton occurs.

As can be seen in Figure 5, there is a strong link between grain size, cooling rate, and $g_{s,perc}$. Firstly, smaller grains have lower values of $g_{s,perc}$. Secondly, $g_{s,perc}$ increases with increasing cooling rate. Thirdly, the effect of grain size on $g_{s,perc}$ is significant for low cooling rates, but not for high cooling rates. These variations in $g_{s,perc}$ are due to back-diffusion within the solid grains. At low cooling rates, the back-diffusion reduces the solid composition at the solid-liquid interface and thus increases the solidification rate. Furthermore, the effect is more pronounced in small grains because the distance for solid diffusion is less. For high cooling rates, however, there is not enough time for back-diffusion to affect the solidification rate, and thus size effects are negligible. For example, with $\dot{T} = 10^{-2}$ °C s^{-1}, $g_{s,perc}$ ranges between $\cong$ 0.81 to 0.97, whereas with $\dot{T} = 10^{2}$ °C s^{-1}, $g_{s,perc}$ >0.99 for all grain sizes.

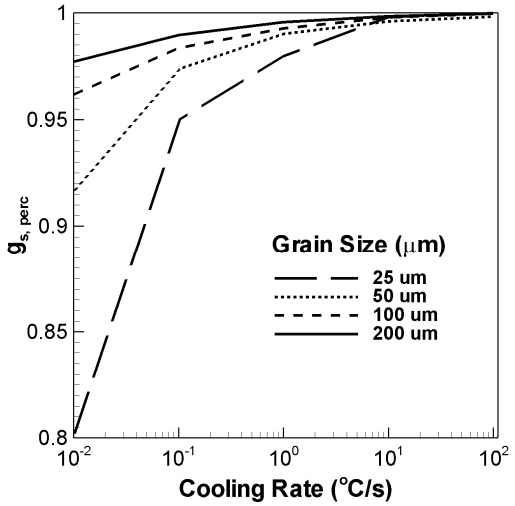

Figure 5: Effects of grain size and cooling rate on $g_{s,perc}$ for a simulation of 1000 grains.

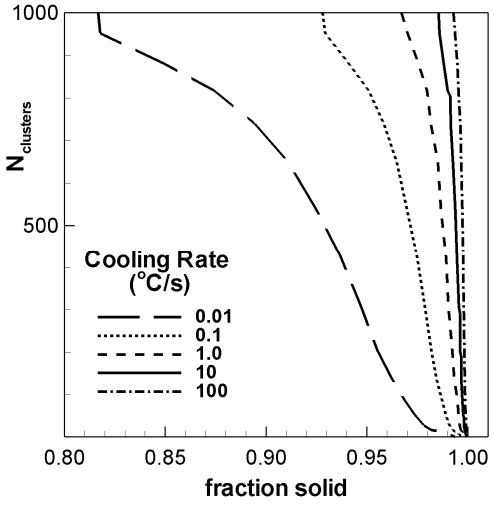

Figure 6: Effect of cooling rate on the evolution of the number of grain clusters.

Formation of Grain Clusters

In Figure 6, the evolution of the number of grain clusters (including isolated grains) as a function of fraction solid has been plotted for five different cooling rates between 0.01 and 100 °C s^{-1}, and for a grain size of 100 μm. Since the 3D simulation was run for 1000 grains, all the curves start at this value and decrease to 1 when all the grains are in physical contact after coalescence. As can be seen in the figure, the start of clustering occurs over a wide range of fraction solid, depending on the cooling rate. For $\dot{T}$ = 0.01 °C s^{-1}, the clustering begins at $g_s \cong 0.82$, whereas for $\dot{T}$ = 100 °C s^{-1}, no clustering occurs until $g_s \cong 0.99$. At this high cooling rate, the results indicate that the decrease in the number of clusters occurs extremely rapidly. In contrast, at the lowest cooling rate, grain clustering occurs over a wide range of fraction solid since the small tetrahedral elements will coalesce before the larger ones. The variation in the evolution of grain clusters is due to the effect of back-diffusion in the solid grains, in a similar manner to the effects of back-diffusion on $g_{s,perc}$. Furthermore, based on this reasoning, small grains will also begin to cluster at lower fraction solid as compared to larger grains. As the clustering of the grains increases ($N_{clusters}$ decreases), so does the cross-sectional area which can sustain ductile deformation. Although the semi-solid does not yet contain a percolated solid network, it is thus able to better withstand tensile strain, reducing the susceptibility to hot tearing.

Conclusions

A new 3D granular solidification model has been developed. Based on the geometry derived from a Voronoi tessellation, the new model takes into account back-diffusion in the solid and thermodynamic coalescence when simulating the evolution of fraction solid with temperature. The 3D model has two main advantages over earlier 2D models. Firstly, the 3D model contains large pockets of liquid whereas the 2D model only contains channels of liquid. These pockets of liquid are important in predicting solidification defects. Secondly, the 3D model allows for simultaneous continuity of the solid and liquid phases across the domain. In 2D, only one phase can be continuous at any specific fraction solid. Hence the 3D model makes improved predictions with respect to solid percolation, and the localization of liquid feeding.

As shown in the results, both cooling rate and grain size have a large effect on the development of the solid network during solidification. Based on this dependence, hot tearing susceptibility will be reduced for material containing small grain sizes. This is because a semi-solid with small grains will have both a small solidification window for strain localization prior to solid percolation, and more grain clustering as compared to a semi-solid with large grains.

Acknowledgements

The authors would like to acknowledge NSERC (Natural Sciences and Engineering Research Council, Canada) and CCMX (Competence Centre for Materials Science and Technology, Switzerland) for financial assistance.

References

1. J. Sengupta, S.L. Cockcroft, D.M. Maijer and A. Larouche, "Quantification of temperature, stress, and strain fields during the start-up phase of direct chill casting process by using a 3D fully coupled thermal and stress model for AA5182 ingots," *Mater Sci Eng A*, 397 (2005), 157-177.
2. B. Commet, P. Delaire, J. Rabenberg and J. Storm, "Measurement of the onset of hot cracking in DC cast billets," *Light Metals 2003*, TMS, (2003), 711-717.
3. I. Farup, M. Rappaz and J.M. Drezet, "In situ observation of hot tearing formation in succinonitrile-acetone," *Acta Mater*, 49 (2001), 1261-1269.
4. H. Fredriksson and B. Lehtinen, "Continuous Observations of Hot Crack-Formation During Deformation and Heating in a Scanning Electron Microscope," *Int Conf Solidification & Casting, Met Soc London*, 2 (1977),
5. D.G. Eskin, Suyitno and L. Katgerman, "Mechanical properties in the semi-solid state and hot tearing of aluminium alloys," *Prog Mater Sci*, 49 (2004), 629-711.
6. Suyitno, W.H. Kool and L. Katgerman, "Hot tearing criteria evaluation for direct-chill casting of an Al-4.5 Pct Cu alloy," *Metall Mater Trans A*, 36A (2005), 1537-1546.
7. M. M'Hamdi, A. Mo and C.L. Martin, "Two-phase modeling directed toward hot tearing formation in aluminum direct chill casting," *Metall Mater Trans A*, 33 (2002), 2081-2093.
8. V. Mathier, J.M. Drezet and M. Rappaz, "Two-phase modelling of hot tearing in aluminium alloys using a semi-coupled approach," *Modell Simul Mater Sci Eng*, 15 (2007), 121-134.
9. D.J. Lahaie and M. Bouchard, "Physical modeling of the deformation mechanisms of semisolid bodies and a mechanical criterion for hot tearing," *Metall Mater Trans B*, 32 (2001), 697-705.
10. W.O. Dijkstra, C. Vuik, A.J. Dammers and L. Katgerman, "Network modeling of liquid metal transport in solidifying aluminium alloys," *Solid Proc & Microst: Symp Hon of W Kurz*, TMS, (2004), 151-156.
11. S. Vernede, P. Jarry and M. Rappaz, "A granular model of equiaxed mushy zones: Formation of a coherent solid and localization of feeding," *Acta Mater*, 54 (2006), 4023-4034.
12. S. Vernede and M. Rappaz, "A simple and efficient model for mesoscale solidification simulation of globular grain structures," *Acta Mater*, 55 (2007), 1703-1710.
13. A.B. Phillion, S.L. Cockcroft and P.D. Lee, "A three-phase model for predicting the effect of microstructural features on semi-solid tensile deformation," *Acta Mater*, 56 (2008), 4328-4338.
14. V.R. Voller and S. Sundarraj, "Modeling of Microsegregation," *Mater Sci Techn*, 9 (1993), 474-481.
15. M. Rappaz, A. Jacot and W.J. Boettinger, "Last-stage solidification of alloys: Theoretical model of dendrite-arm and grain coalescence," *Metall Mater Trans A*, 34 (2003), 467-479.
16. T.W. Clyne and G.J. Davies, "The Influence of Composition on Solidification Cracking Susceptibility in Binary Alloy Systems," *Br Foundryman*, 74 (1981), 65-73.
17. J. Campbell. *Castings*. (Schaumburg, IL: Butterworth Heinemann, 2003).
18. Suyitno, D.G. Eskin, V.I. Savran and L. Katgerman, "Effects of alloy composition and casting speed on structure formation and hot tearing during direct-chill casting of Al-Cu alloys," *Metall Mater Trans A*, 35A (2004), 3551-3561.